UNIVERSITÀ DEGLI STUDI DI PADOVA

Dipartimento di Fisica e Astronomia "Galileo Galilei"

Corso di Laurea in Fisica

Tesi di Laurea

Conformal transformations of orbital angular momentum beams

Relatore

Dott. Gianluca Ruffato

Laureando

Pietro Maria Sanguin

Anno Accademico 2020/2021

Dedicated to my family

Abstract

In this thesis we will discuss the role of conformal transformations in modern optics and their link with the Laplace equation. We will start from the classical derivation of the Fresnel-Kirchhoff diffraction integral which we will rewrite, thanks to the Fourier transform, into a form more suitable for computer simulation. Then we are going to describe what are the main features of a beam carrying orbital angular momentum (OAM) and the general Laguerre-Gaussian (LG) beams equation in polar coordinates, as a prototypal example of OAM beams. In the core of the thesis we will discuss which kind of transformations are applicable to OAM beams, then we will study two particular types of transformations, i.e., the logarithmic-polar and the circular-sector mappings, which have a fundamental role in the optical manipulation of OAM beams. In particular, the functionalities studied are (de)multiplexing, i.e., sorting (and generation) of OAM beams, and the n-fold multiplication of a given OAM beam. We are going to present also some MATLAB simulations of both applications.

Notation

The following abbreviations will be used:

OAM Orbital angular momentum

LG Laguerre-Gaussian

CST Circular-sector transformation

IR Impulse response

TF Transfer function

SAM Spin angular momentum

SPA Stationary phase approximation

Contents

1 Introduction

Light can behave, in all its spectrum, both as a particle and as a wave. This feature has been observed, for instance, through the photoelectric effect and the diffraction pattern in Young's double slit experiment, respectively. Maxwell (theoretically) and Hertz (experimentally) proved that the light waves are formed of two swinging fields that do not need a medium to propagate. The wave-like behavior is shared also by all the subatomic particles. The mathematical description of this kind of waves shares the material point features, such as the angular momentum, together with the wave characteristics such as the phase. Indeed the angular momentum is $\vec{L} = \vec{r} \times \vec{p}$ where $\vec{r}$ is the position, $\vec{p}$ is the linear momentum, clearly this definition is not immediately practical for describing a wave as it does not have a definite position in space. A wave spreads in space and it is repetitive, therefore it is better described by a periodic function. This periodic function of a certain real variable t (such as time) has a phase which is an angle-like quantity representing the fraction of the cycle covered up to t. As we will see, OAM is rather related to the spatial phase structure of phase fronts, and we will consider how to manipulate OAM by altering the phase distribution of a wavefield with conformal transformations.

1.1 Elements of Diffraction Theory

A field $U(\vec{r}, t)$ that satisfies the d'Alembert equation:

$$\Box U = 0 \qquad \Box = \nabla^2 - \frac{1}{c^2}\frac{\partial^2}{\partial t^2} \tag{1.1}$$

obeys the wave equation and therefore propagates itself as a wave of speed c. The monochromatic solution is $U(\vec{r}, t) = a(\vec{r})\cos(\phi(\vec{r}) - \omega t)$ that could be written smartly as:

$$U(\vec{r}, t) = U(\vec{r})e^{-i\omega t} \qquad U(\vec{r}) = a(\vec{r})e^{i\phi(\vec{r})} \tag{1.2}$$

where $U(\vec{r})$ is the complex amplitude. If we put this field into the wave equation we get the Helmholtz equation:

$$\nabla^2 U(\vec{r}, t) = -k^2 U(\vec{r}, t) \tag{1.3}$$

where $k = \frac{2\pi}{\lambda}$ is the wavenumber and λ is the wavelength. A particular solution of this equation has the complex amplitude:

$$U(\vec{r}) = \frac{A_0}{r}e^{ikr} \tag{1.4}$$

The latter equation represents a spherical wave which propagates from a source in the origin. The Huygens-Fresnel principle states that every point reached from a point source in the origin of the reference frame is a source itself of spherical waves

whose envelope generates the new wave front. Let S (figure 1.1) be the instantaneous position of a spherical monochromatic wave-front of radius r_0 with a point source P_0, and let P be a point where the light disturbance is to be determined [2][1]. With this notation the mathematical translation of the Huygens-Fresnel principle is:

$$U(P) = U_0 \iint_S \frac{e^{iks}}{s} K(\chi) dS \tag{1.5}$$

where U_0 is the disturbance at a point Q on the wave-front, $\vec{s} = QP$, $K(\chi)$ is the obliquity factor which describes the variation with the direction of the amplitude of the secondary waves and χ in the angle between the normal at Q and $\vec{s}$. The obliquity factor was not present in the original Fresnel-Huygens theory, but appears explicitly in the Kirchhoff's diffraction theory explaining the experimental data. In fact the Huygens-Fresnel principle alone is lacking because it also allows, for instance, backward propagation with respect to the original propagation direction.

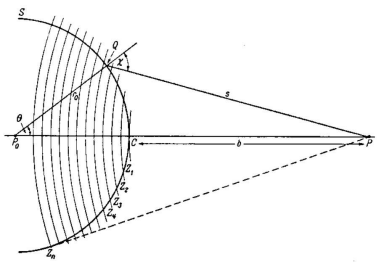

Figure 1.1

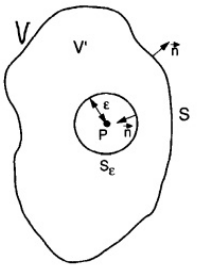

Figure 1.2

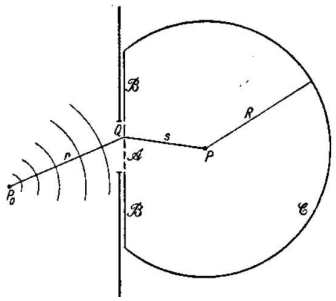

Figure 1.3

Our aim is to obtain a pointwise formula that describes the field after passing through a diffractive element. The rigorous way to achieve this result is the Kirchhoff's diffraction theory. Now if we take a volume V surrounding a point of observation P as in figure 1.2, how do we express the optical disturbance at P in terms of its values on the surface S? To achieve this goal we begin with the Green's Formula:

$$\iiint_V (U\nabla^2 G - G\nabla^2 U) dV = \iint_S \left(U\frac{\partial G}{\partial n} - G\frac{\partial U}{\partial n} \right) dS \tag{1.6}$$

where $\frac{\partial}{\partial n}$ indicates a partial derivative in the outward normal direction at each point on S and assuming that U, G, and their first and second partial derivatives are continuous within and on S. If we choose as a function $G(s) = \frac{e^{iks}}{s}$ it is clear that it satisfies the conditions of the Green's Formula and also equation (1.3). Now thanks to our choice of the function we can combine (1.3) and (1.6), obtaining [6][2]:

$$\iint_S \left(U\frac{\partial G}{\partial n} - G\frac{\partial U}{\partial n} \right) dS = 0 \tag{1.7}$$

Clearly the function $G(s)$ has a singularity for $s = 0$, and since G was assumed to be continuous and differentiable, P must be excluded from the domain of integration. We exclude the discontinuity at P, with a small spherical surface S_ϵ of radius ϵ. Then we have:

[1] Ivi p. 371

[2] Ivi chapter 3 pp. 41-45

$$\iint_{S+S_\epsilon} \left[\frac{\partial U}{\partial n}\frac{e^{iks}}{s} - U\frac{\partial}{\partial n}\left(\frac{e^{iks}}{s}\right)\right] dS = 0 \tag{1.8}$$

Evaluating the integral around S_ϵ, considering the limit for $\epsilon \to 0$ and evaluating the integral pointwise we get to the Integral Theorem of Helmholtz and Kirchhoff:

$$U(P) = \frac{1}{4\pi}\iint_S \left[\frac{\partial U}{\partial n}\frac{e^{iks}}{s} - U\frac{\partial}{\partial n}\left(\frac{e^{iks}}{s}\right)\right] dS \tag{1.9}$$

that evaluates the disturbance at P. Now if we look at figure 1.3 and we consider a spherical wave, emitted from P_0, hitting the foil, it is possible to introduce a convenient surface in order to apply (1.9). Part $\mathcal{A}$ is the aperture, part $\mathcal{B}$ is the non illuminated screen and $\mathcal{C}$ is the large sphere used to have a close surface around the observation point P. Then, we apply the Kirchhoff's boundary conditions. Therefore on $\mathcal{A}$:

$$U = U^{(i)} \qquad U^{(i)} = \frac{A_0 e^{ikr}}{r} \qquad \frac{\partial U^{(i)}}{\partial n} = \cos(n,r)\left(ik - \frac{1}{r}\right)\frac{A_0 e^{ikr}}{r} \tag{1.10}$$

Whereas on $\mathcal{B}$ the field and its derivative are zero and on $\mathcal{C}$ happens the same because of considering $R \to \infty$ and that the radiation field does not exists at all times but that it is produced by a source that begins to radiate at a certain particular instant of time. We can now use (1.9) on the surface $\mathcal{A}$ and if we take $R \to \infty$ and we neglect in the normal derivatives the terms $1/r$ and $1/s$ in comparison to k, we get to the Fresnel-Kirchhoff diffraction formula [2][3]:

$$U(P) = -\frac{iA_0}{2\lambda}\iint_A \frac{e^{ik(r+s)}}{rs}[\cos(n,r) - \cos(n,s)]dS \tag{1.11}$$

where (n,r) is the angle between r and the surface's normal vector. Setting $\chi = \pi - (r,s)$ we obtain $K(\chi) = \frac{1}{2i\lambda}(1+\cos\chi)$ which is the obliquity factor. For the rest of the thesis we will use a more general form of (1.11), indeed our interest is to describe the change of the field when it passes through a diffractive element. Assuming that the distances of the source and of the point P are large compared to the typical size of the aperture, then $\cos(\chi) \approx 1$ and the obliquity factor reduces to $1/(i\lambda)$. The resulting form of the Fresnel-Kirchhoff diffraction formula is:

$$U(P) = \frac{1}{i\lambda}\iint_A U^i(P')A(P')\frac{e^{ikr}}{r}dS \tag{1.12}$$

where $U^i(P')$ is the input field and $A(P')$ is the aperture function. In $A(P')$ it is stored the whole information about the shape and transmission of the diffractive element and the term r is the distance between the point of input field P' and the arrival point of the field P. If we suppose to span two planes with $P' \in x\hat{O}y$, $P \in u\hat{O}v$ and a z axis pointing from $x\hat{O}y$ to $u\hat{O}v$ as in figure 1.4 we can write the distance between the two points and approximate it using Taylor expansion as [17]:

$$r = z\sqrt{1 + \frac{(u-x)^2 + (v-y)^2}{z^2}} \qquad r \approx z + \frac{(u-x)^2}{2z} + \frac{(v-y)^2}{2z} \tag{1.13}$$

[3]Ivi pp. 379-380

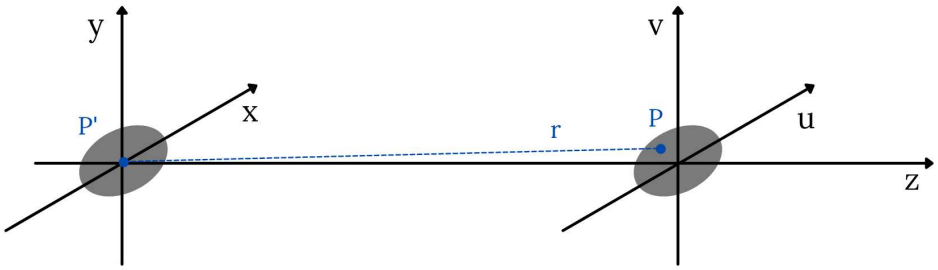

Figure 1.4: Frame references for the Fresnel-Kirchhoff diffraction formula in Eq. (1.14)

Applying this paraxial approximation, also called Fresnel approximation, to (1.12) and neglecting the terms of order greater than two we have:

$$U(u,v) = \frac{e^{ikz}}{i\lambda z} \iint_A U^i(x,y) A(x,y) e^{ik\left(\frac{(u-x)^2}{2z} + \frac{(v-y)^2}{2z}\right)} dxdy \tag{1.14}$$

The previous integral is a convolution integral, which can be written as:

$$U(u,v) = \iint_A U^i(x,y) A(x,y) h(u-x, v-y) dxdy = \left[(U^i A) * h\right](u,v) \tag{1.15}$$

where $h(u,v)$ is called impulse response function and in cylindrical coordinates is given by:

$$h(\rho, z) = \frac{e^{ikz}}{i\lambda z} e^{\frac{ik}{2z}\rho^2} \qquad \rho = \sqrt{u^2 + v^2} \tag{1.16}$$

Now we can apply the Fourier convolution theorem[4] to (1.15) getting[5]:

$$U(u,v) = \mathcal{F}^{-1}\left\{\mathcal{F}\{U^i A\}\mathcal{F}\{h\}\right\} \tag{1.17}$$

For the numeric computation of the field, under some conditions (see A.4), it is better to use the analytic expression of $H(f_u, f_v) = \mathcal{F}\{h(u,v)\}$ which is called transfer function. In particular:

$$H(f_u, f_v) = e^{ikz} e^{-i\pi\lambda z(f_u^2 + f_v^2)} \tag{1.18}$$

[4] $\mathcal{F}\{f * g\} = \mathcal{F}\{f\} \cdot \mathcal{F}\{g\}$

[5] In general a 2D Fourier transform is $\mathcal{F}[g(x,y)](f_x, f_y) = \iint g(x,y) e^{-i2\pi(xf_x + yf_y)} dxdy$.

1.2 What is an OAM beam?

Light transports both energy and momentum. The momentum may have a linear and an angular component, as it exerts radiation pressure and torque on objects. Quantitatively the angular momentum density of an electromagnetic field is [1]:

$$\vec{\mathcal{L}} = \epsilon_0 \vec{r} \times (\vec{E} \times \vec{B}) \tag{1.19}$$

since the linear momentum density is: $\vec{p} = \epsilon_0 \vec{E} \times \vec{B}$. The angular momentum of light is made up of a spin part, spin angular momentum (SAM), associated with polarization and an orbital part (OAM) associated with spatial distribution. The spin part or spin angular momentum, from the quantum theory, has two states $\pm\hbar$ corresponding to right-handed and left-handed circular polarisations, whereas the OAM has infinite discrete states $\pm\ell\hbar$ because ℓ is an integer value. It is clear that the OAM could be order of magnitude higher than the SAM. The total angular momentum of the field is:

$$\vec{J} = \epsilon_0 \int \vec{r} \times (\vec{E} \times \vec{B}) d\vec{r} \tag{1.20}$$

and in the paraxial approximation holds true: $\vec{J} = \vec{L} + \vec{S}$. One of the first seminal work on this topic [1] shows that laser light with a Laguerre-Gaussian amplitude distribution has a well defined OAM. The Laguerre-Gaussian beam is not the only one which carries OAM, other examples are: Bessel, Bessel–Gauss, Hermite–Gauss, and Mathieu beams [4]. For our purposes we will focus on the Laguerre-Gaussian beam. This kind of OAM beams derives directly from the Helmholtz equation in the paraxial approximation. Changing to cylindrical coordinates (r, θ, z), equation (1.3) becomes:

$$\nabla_\perp^2 U + \left(\frac{\partial^2 U}{\partial z^2}\right) + k^2 U = 0 \quad \text{with} \quad \nabla_\perp^2 = \frac{1}{r}\frac{\partial}{\partial r}\left(r\frac{\partial}{\partial r}\right) + \frac{1}{r^2}\left(\frac{\partial^2}{\partial \theta^2}\right) \tag{1.21}$$

A paraxial wave can be described with a complex envelope $X(\vec{r})$ which is a slowly varying function of position z in the propagation direction so that the complex amplitude of the wave becomes $U(\vec{r}) = X(\vec{r})e^{ikz}$. The variation of the envelope X and its derivative with z must be slow within the distance of a wavelength, so that the wave approximately maintains its underlying plane-wave nature $\left|\frac{\partial^2 X}{\partial z^2}\right| \ll \nabla_\perp^2 X$. Substituting in Eq. (1.21) we have:

$$\nabla_\perp^2 X + 2ik\frac{\partial X}{\partial z} = 0 \tag{1.22}$$

By solving equation (1.22) in different coordinate systems with different symmetry assumptions, we can define several families of beams that carry OAM. If we assume the problem is cylindrically symmetric and use cylindrical coordinates (r, θ, z) the LG beam can be realized as[6] [4]:

$$\begin{aligned} U_{\mathrm{LG}(p,\ell)}(r,\theta,z) =& \frac{C_{\mathrm{LG}(p,\ell)}}{w(z)}\left(\frac{r\sqrt{2}}{w(z)}\right)^{|\ell|} L_p^{|\ell|}\left(\frac{2r^2}{w^2(z)}\right)\exp\left[\frac{-r^2}{w^2(z)} - \frac{ikr^2 z}{2\left(z^2 + z_R^2\right)}\right] \\ & \times \exp[i(2p + |\ell| + 1)\zeta(z)]\exp(i\ell\theta)e^{ikz} \end{aligned} \tag{1.23}$$

[6] See appendix A.5

where w_0 is the beam waist. In the previous equation the factor $\exp(i\ell\theta)$ states the existence of beams characterized by $|\ell|$ helical wave fronts twisting clockwise or counterclockwise depending on the sign of ℓ. The intensity distribution exhibits a ring shape around a central dark singularity on a plane perpendicular to the propagation axis. OAM beams therefore have an azimuthal phase gradient (see Figure 1.5). The radial number p defines the number of concentric intensity rings, equal to $(p+1)$. In the following, we will limit ourselves to the case $p = 0$, since we are interested only in the OAM degree of freedom.

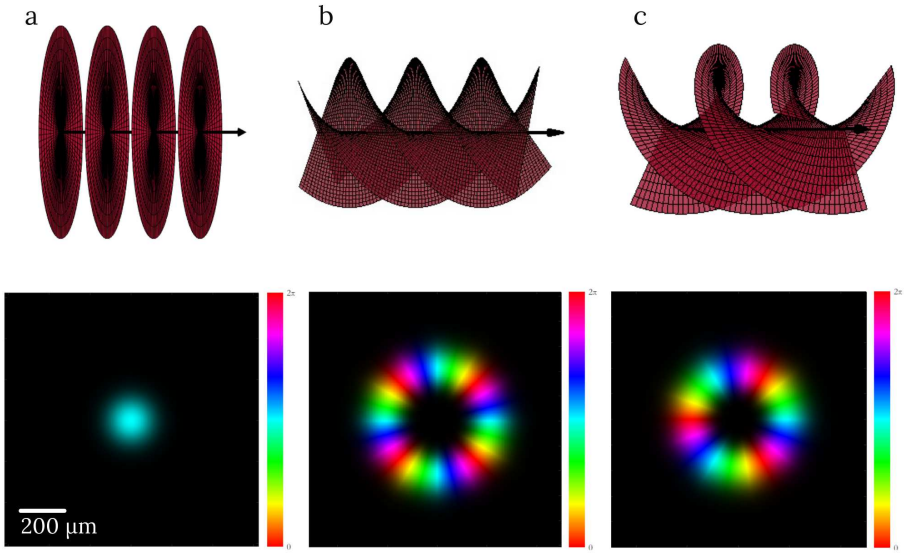

Figure 1.5: $\mathrm{LG}_{(p,\ell)}$ beam phase and intensity with $w_0 = 150$ μm at $z = 0$ μm (a) $\mathrm{LG}_{(0,0)}$ (b) $\mathrm{LG}_{(0,4)}$ (c) $\mathrm{LG}_{(0,-3)}$. Brightness and colours refer to intensity and phase, respectively.

2 Conformal optical transformations

2.1 Optical and conformal trasformations

In the introduction we showed that the diffraction integral in the paraxial approximation:

$$U(u,v) = \frac{e^{ikz}}{i\lambda z} e^{\frac{ik}{2z}(u^2+v^2)} \iint_A U^i(x,y) A(x,y) e^{ik\left(\frac{x^2+y^2}{2z} - \frac{(ux+vy)}{z}\right)} dxdy \tag{2.1}$$

describes, in the paraxial regime, the propagation of an optical wave after passing through a phase-shaping region, where the starting plane is $x\hat{O}y$ and the wave propagates up to the arrival plane $u\hat{O}v$. Now the question is: what conditions must the integral respect to converge? For $k \to \infty$ we have λ approaching zero which is the case of common physical problems. Under this hypothesis the answer is given by the stationary phase approximation (SPA). The SPA consists in approximating the integral with the values of the integrand in the stationary points of Φ (defined

later), i.e., those that satisfy the gradient condition $\nabla\Phi = 0$[1]. Defining $A(x, y)$ as a phase element:

$$A(x, y) = \exp(i\Omega(x, y)) \quad \text{with} \quad \Omega(x, y) = \Omega'(x, y) - k\frac{x^2 + y^2}{2f} \tag{2.2}$$

we are interested in solving the integral in $z = f$:

$$\Phi(x, y) = \frac{\Omega'(x, y)}{k} - \left(\frac{xu + yv}{f}\right) \tag{2.3}$$

While it is straightforward to apply the SPA, our purposes are to find the conditions of convergence for the integral in Eq. (2.1). We are not interested in the analytical solution, finding the conditions of convergence is enough. There is a more practical way to rewrite the latter equation, in fact stating $\vec{\mathfrak{u}} = (u, v)$ and $\vec{\mathfrak{r}} = (x, y)$ we have:

$$\Phi(x, y) = \frac{\Omega'(x, y)}{k} - \left(\frac{\vec{\mathfrak{u}} \cdot \vec{\mathfrak{r}}}{f}\right) \tag{2.4}$$

and applying the last condition of integral's convergence $\nabla\Phi = 0$ (condition of stationary phase) we obtain:

$$\nabla\Omega' = k\frac{\vec{\mathfrak{u}}}{f} \tag{2.5}$$

This equation expresses the link between the optical element inducing the transformation and the coordinates on the destination plane [15]. We remind that a gradient is always irrotational and therefore it must be $\nabla \times \vec{\mathfrak{u}} = \vec{0}$, computing that product we get to $(0, 0, \partial_x v - \partial_y u) = \vec{0}$ thus:

$$\frac{\partial u}{\partial y} = \frac{\partial v}{\partial x} \tag{2.6}$$

For the purpose of OAM optical processing, we are looking for a transformation which locally conserves the angles, i.e., it is conformal. A conformal mapping can be holomorphic[2] or anti-holomorphic. The condition (2.6) suggests the choice of an anti-holomorphic mapping, therefore:

$$\frac{\partial u}{\partial x} = -\frac{\partial v}{\partial y} \tag{2.7}$$

must be satisfied. Equations (2.6) and (2.7) are the so-called Cauchy-Riemann conditions. Taking the divergence of (2.5) and substituting the latter two conditions we get the Laplace equation:

$$\nabla^2\Omega' = 0 \tag{2.8}$$

[1]Reported completely in appendix A.1

[2]See appendix A.2

Hence, the phase function of an optical element performing an anti-holomorphic (conformal) transformation must be harmonic. After using the SPA, the field results:

$$U(u,v) \approx \sum_{x_0,y_0 \in \Sigma} \frac{2\pi\sigma}{\lambda z} e^{ikz} \frac{U^{(i)}(x_0,y_0)}{\sqrt{|H|}} e^{i\Phi(x_0,y_0)} \tag{2.9}$$

where $H = \det(\mathrm{Hess}(\Phi))$, Σ is the set of nondegenerate critical points and $\sigma = \mathrm{sgn}(\partial^2\Phi/\partial x^2)$ when $H > 0$, $\sigma = -i$ otherwise. From Eq. (2.9) it is evident that the field has still a proper phase component $\exp(i\Phi(x_0,y_0))$, that must be nullified to achieve our purpose of phase transformation. In order to do that, it is used a second phase element, called phase-corrector, located in the $u\hat{O}v$ plane (see figure 1.4), so that:

$$\Omega_{PC}(u,v) = -\Phi(x_0,y_0) \tag{2.10}$$

with (x_0,y_0) the nondegenerate critical points of Φ. Sometimes the conformal transformations with two-elements are said Hossack's transformations due to his early work on them [7]. A general real solution[3] of (2.8) in polar coordinates (r,θ) is given by:

$$\Omega'(r,\theta) = Ar^m \cos(m\theta + \theta_0) \tag{2.11}$$

Now the question is: what kind of transformations are allowed to be done with two confocal harmonic elements? In the following sections, we will focus on two of the most important conformal mappings exploited in the framework of structured light for OAM beams manipulation. In particular, the optical transformation and propagation of OAM beams will be simulated and calculated at different z-positions implementing the convolution algorithm in equation (1.17).

3 Logarithmic-Polar transformation

3.1 The log-pol transformation

A specific map that obeys the latter conditions is the logarithmic-polar transformation. Such transformation is used to generate a phase linearization in the case of an azimuthal phase gradient in input. The analytic form of this kind of transformation, in polar coordinates, is:

$$\vec{\mathfrak{u}} = \begin{cases} u = -a\log\left(\frac{r}{b}\right) \\ v = a\theta \end{cases} \tag{3.1}$$

where a and b are scaling and translation parameters, respectively. The parameter $a = L/2\pi$ ensures that the azimuthal angle range is mapped onto a length L shorter than the full width of the second element. The parameter b is optimized for the particular physical dimensions of the sorter and can be chosen independently [16]. In the log-pol mapping, the first optical element is called unwrapper and the second

[3] See appendix A.3

phase corrector. Now we see our previous considerations about optical transformations at work. The field in the image plane with an input OAM beam after the unwrapper is:

$$U(u,v) = \frac{e^{ikz}}{i\lambda z} e^{\frac{ik}{2z}(u^2+v^2)} \iint_A U_{LG} e^{i\Omega_S} e^{ik\left(\frac{x^2+y^2}{2z} - \frac{(ux+vy)}{z}\right)} dxdy \tag{3.2}$$

where Ω_S is analytical form of the 2D phase that the unwrapper has to convey to the field, which is defined in (2.2). Hence the total phase Φ is equal to (2.3). Thanks to (2.5), we are now able to calculate the analytical form of the phase element for $z = f$, indeed in Cartesian coordinates we get:

$$\left(\frac{\partial \Omega'_S}{\partial x}, \frac{\partial \Omega'_S}{\partial y}\right) = \frac{ak}{f}\left(-\log\left(\frac{\sqrt{x^2+y^2}}{b}\right), \arctan\left(\frac{y}{x}\right)\right) \tag{3.3}$$

Computing a primitive of this vector field results in:

$$\Omega'_S(x,y) = \frac{ak}{f}\left(y\arctan\left(\frac{y}{x}\right) - x\log\left(\frac{\sqrt{x^2+y^2}}{b}\right) + x\right) \tag{3.4}$$

and therefore

$$\Omega_S(x,y) = \frac{ak}{f}\left(y\arctan\left(\frac{y}{x}\right) - x\log\left(\frac{\sqrt{x^2+y^2}}{b}\right) + x\right) - k\frac{x^2+y^2}{2f} \tag{3.5}$$

where the last term is a focusing factor. The phase corrector (2.10) is obtained from:

$$\Omega_{PC}(u,v) = -\frac{\Omega'_S(x_0,y_0)}{k} + \left(\frac{x_0 u + y_0 v}{f}\right) \tag{3.6}$$

where x_0 and y_0 are the inverse of (3.1) in polar coordinates [1]. Easy calculations get to:

$$\Omega_{PC}(u,v) = -\frac{abk}{f} e^{-\frac{u}{a}} \cos\left(\frac{v}{a}\right) - k\frac{u^2+v^2}{2f} \tag{3.7}$$

L	λ	a	b	f [mm]
2000	0.6328	200	250	20

Table 3.1: Physical parameters in μm of the log-pol simulation in Fig. 3.1

The parameter L is the length of the simulation square been sampled in $M = 1000$ pixels. For every pixel of width $dx = L/M$ the intensity $I = |U(u,v)|^2$ and the phase are calculated obtaining the previous images. The presented propagation has the unwrapper at $z = 0$ and the phase corrector at $z = f$. The final wave is slightly distorted as the calculation of the optical phases assumes plane waves without OAM which instead are used in the simulation.

[1] Respectively $x_0 = be^{-\frac{u}{a}} \cos\left(\frac{v}{a}\right)$ and $y_0 = be^{-\frac{u}{a}} \sin\left(\frac{v}{a}\right)$

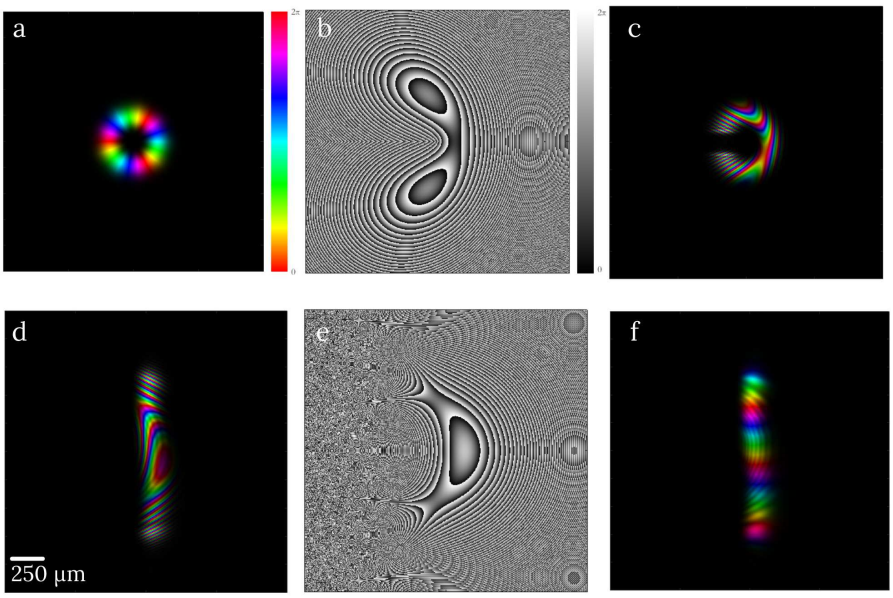

Figure 3.1: (a) Input $\mathrm{LG}_{(0,3)}$, $w_0 = 150\ \mu$m, (b) unwrapper phase pattern, (c) beam at $z = 0.1f$, (d) $z = f$, (e) phase-corrector phase pattern, (f) after the phase-corrector. For the transformation parameters see Table 3.1. In (a, c ,d ,f) brightness and colours refer to intensity and phase, respectively.

Sampling regimes

The Shannon–Nyquist sampling theorem states that to resolve all frequencies in a function, it must be sampled at least twice the highest frequency present. This theorem must be respected in the numerical simulations to avoid aliasing and artifacts. As shown in the introduction a field can be propagated using either the impulse response (IR) (1.16) or the transfer function (TF) (1.18). The numerical implementation varies depending on the choice of the IR or TF. In fact as shown in [17] the results are influenced by the chosen sampling[2]. A parameter[3] [13]:

$$c = \frac{\lambda z}{Ldx} \tag{3.8}$$

can be defined to identify which regime is more suitable to describe the propagation at a given distance z. The critical sampling condition in which the two functions produce the same result occurs when c=1, in the other cases we have that one is more exact than the other:

$$\begin{cases} c > 1 & \text{IR} \\ c < 1 & \text{TF} \end{cases} \tag{3.9}$$

3.2 OAM-mode division multiplexing

An application of the log-pol transformation consists in assembling a detector capable of measuring the topological charge ℓ, and therefore the OAM, of any light beam. If immediately after the phase corrector we put a lens of focal length F it

[2]Chapter 5
[3]See Appendix A.4

will focus the input intensity field into a single elongated spot in its focal plane. In general the transmission function (input plane) of a lens is:

$$A(x,y) = e^{-ik\frac{x^2+y^2}{2F}} \tag{3.10}$$

Using this result inside (2.1) we can calculate the field at the focal length $z = F$ getting:

$$U(u,v) = \frac{e^{ikF}}{i\lambda F} e^{ik\frac{u^2+v^2}{2F}} \mathcal{F}\{U^i A\} \tag{3.11}$$

Since the input field is: $U^i \sim e^{i\ell\frac{v}{a}}$, the resulting field after the lens is:

$$U(u,v) \sim \delta(\frac{\ell}{a} - \frac{k}{F}v) \tag{3.12}$$

resulting, as expected, in a single spot located at the coordinate:

$$v_\ell = \frac{F\ell}{ak} \tag{3.13}$$

Therefore, the transverse position of this spot is dependent on the OAM state of the input beam which can be analysed in its OAM components. In [10] eleven pure OAM states, $\ell \in [-5, 5]$, were analyzed giving an experimental demultiplexing proof. It is interesting to notice that such experimental apparatus can be used in reverse (multiplexer) as shown in [16]. The numeric calculations of the intensity is made with the same parameters of the log-pol with ($F = 10$cm) and $\ell \in [-7, 7]$ which is varied to study the demultiplexer behaviour. The light spot, for the positive ℓ, is shown in figure 3.2 where the two white lines indicates $v = 0$ and the expected position (3.13). In figure 3.3 we present the intensity distribution after the lens (blue

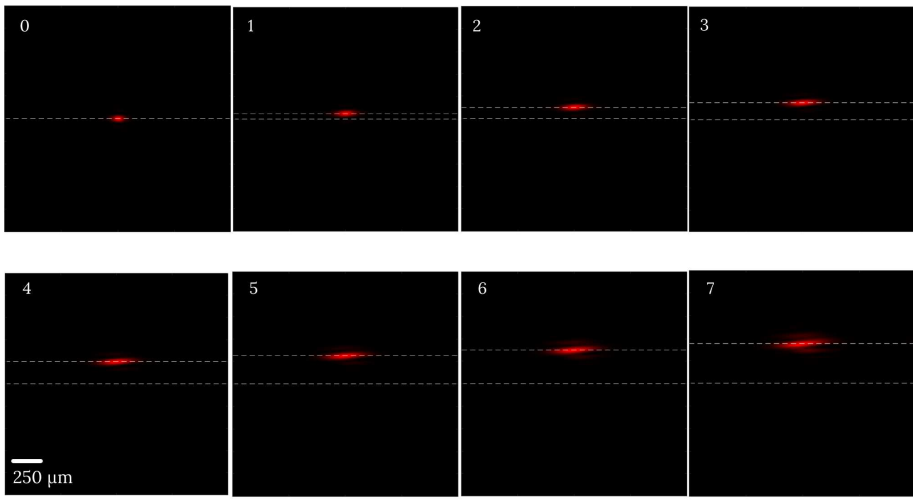

Figure 3.2: Intensity on the back focal plane of the lens for input OAM equal to 0, 1,..., 7

curve) and a Gaussian fit (3.14) (red curve) made around the intensity peak with the function:

$$v = Ae^{-\frac{(u-\mu)^2}{2\sigma^2}} \tag{3.14}$$

The fit is made using the data greater than 40% of the intensity peak. Moreover, figure 3.3 represents the vertical cross-section at the maximum value of the intensity

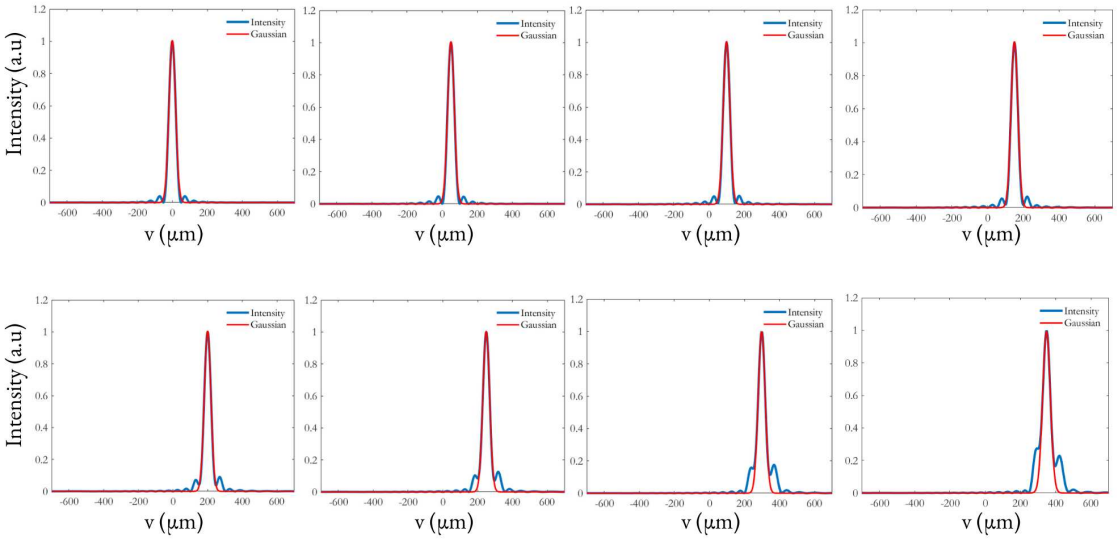

Figure 3.3: Intensity cross-section (blue) and Gaussian fit (red)

OAM ℓ	0	1	2	3	4	5	6	7
A (a.u.)	1	1	1	1	1	1	1	1
μ (μm)	0	50	100	150	200	249	298	347
σ (μm)	19	19	19	19	19	19	20	22

Table 3.2: Gaussian fit results, $\ell \geq 0$

OAM ℓ	-1	-2	-3	-4	-5	-6	-7
A (a.u.)	1	1	1	1	1	1	1
μ (μm)	-50	-100	-150	-200	-249	-298	-347
σ (μm)	19	19	19	19	19	20	22

Table 3.3: Gaussian fit results, $\ell < 0$

and shows the position of the intensity peak. The intensity cross-section profile is globally like a $\mathrm{sinc}(v)$. Similar plots are done for the negative values of ℓ. The results of the fit are shown in Table 3.2 and 3.3 .

It is possible to verify formula (3.13) making a linear regression of the previous results, as shown in figure 3.4. It results $\frac{F}{ak} = (49.8 \pm 1.2)\mu$m which is compatible with the expected $\frac{F}{ak} = 50.4$ μm. To evaluate the output crosstalk of this system we divided the output plane in several horizontal rectangular slices centered at v_ℓ and with $v_\ell/2$ width. Computing the intensity of each ℓ-channel we have the efficiency matrix (figure 3.5), where it is clear that input channels corresponding to $\ell = 7$ and -7 have a higher dispersion producing an output signal also in the neighbouring channels. The percentage of intensity is computed as the ratio between the intensity in the area $-v_\ell/2 < v_\ell < v_\ell/2$ and the total intensity on the plane. In figure 3.6 we show the cross-talk, computed as:

$$XT_{\ell=\ell^*} = 10 \log_{10} \left(\frac{I_{ALL-\ell^*}}{I_{ALL}} \right) \tag{3.15}$$

where I_{ALL} is the signal in correspondence of channel ℓ^* when all input OAM signals are on, while $I_{ALL-\ell^*}$ is the signal at channel ℓ^* when the input channel ℓ^* is off. The average cross-talk is (-5.2 ± 0.2) dB.

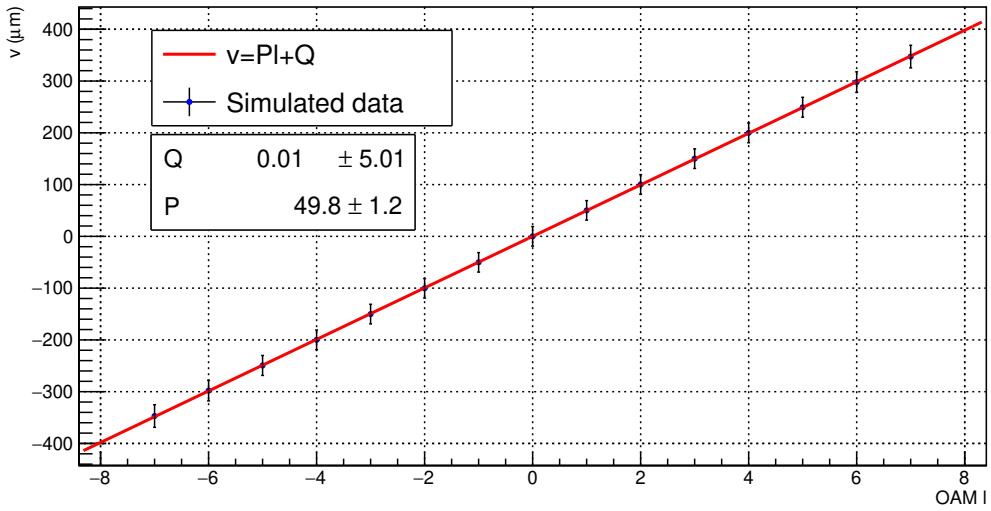

Figure 3.4: Linear regression of the intensity peak position as a function of the input OAM

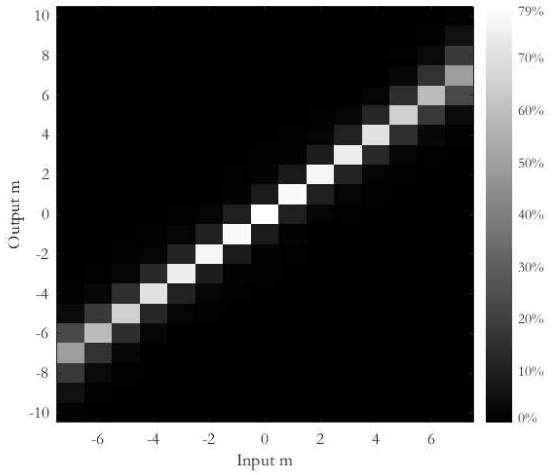

Figure 3.5: Efficiency matrix

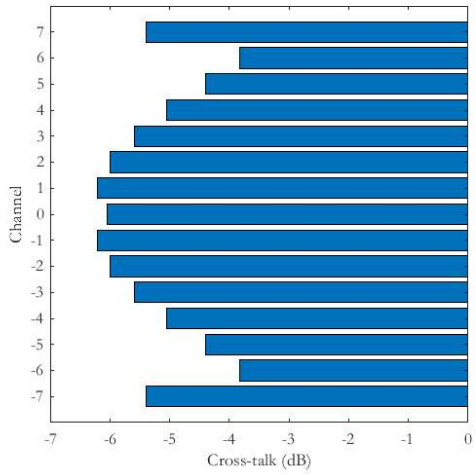

Figure 3.6: Cross-talk

4 Circular-Sector transformation

4.1 The circular-sector transformation

An other mapping that obeys the conditions (2.8) is the circular-sector transformation (CST). This kind of transformation consists in an azimuthal phase scaling. Transforming the Cartesian coordinates for the first and second plane $(x, y) \to (v, u)$ in polar coordinates $(r, \theta) \to (\rho, \varphi)$ we want our transformation to scale the initial whole circle of angular length 2π into a circular sector of $2\pi/n$. The solution to our purpose is to impose:

$$\varphi = \frac{\theta}{n} \tag{4.1}$$

where n is, clearly, the scaling factor. Imposing the transformation to be anti-holomorphic, (Cauchy-Riemann conditions in Eqs. (2.6) and (2.7)), we obtain the

vector in the far field:

$$(\rho, \varphi) = \begin{cases} \rho = a \left(\frac{r}{b}\right)^{-\frac{1}{n}} \\ \varphi = \frac{\theta}{n} \end{cases} \tag{4.2}$$

with a and b being scaling parameters. The diffracted field (2.1) of an input OAM beam, calculated in paraxial approximation and polar coordinates, after passing the first optical element (transformer) located at $z = 0$ results [5]:

$$U(\rho, \varphi) = \frac{e^{ikf}}{i\lambda f} e^{\frac{ik\rho^2}{2f}} \iint_A U_{LG} e^{i\Omega_{Sn}} e^{ik\frac{r^2}{2f}} e^{-ik\frac{r\rho}{f}\cos(\theta-\varphi)} r dr d\theta \tag{4.3}$$

We look for the saddle points of the phase function:

$$\Phi(r, \theta) = \Omega_{Sn}(r, \theta) + k\frac{r^2}{2f} - k\frac{r\rho}{f}\cos(\theta - \varphi) \tag{4.4}$$

Imposing $\nabla\Phi = 0$ and substituting 4.2 we obtain:

$$\left(\frac{\partial\Omega_{Sn}}{\partial r}, \frac{\partial\Omega_{Sn}}{\partial\theta}\right) = \frac{ka}{f}\left(\frac{r}{b}\right)^{-\frac{1}{n}} \left[\cos\left(\theta - \frac{\theta}{n}\right) - \frac{r}{a}\left(\frac{r}{b}\right)^{\frac{1}{n}}, -r\sin\left(\theta - \frac{\theta}{n}\right)\right] \tag{4.5}$$

From that it is straightforward to calculate the analytic form of the transformer and phase-corrector getting:

$$\Omega_{Sn}(r, \theta) = \frac{kab}{f}\left(\frac{r}{b}\right)^{1-\frac{1}{n}} \frac{\cos\left[\left(1 - \frac{1}{n}\right)\theta\right]}{1 - \frac{1}{n}} - k\frac{r^2}{2f} \tag{4.6}$$

$$\Omega_{PC}(\rho, \varphi) = \frac{kab}{f}\left(\frac{\rho}{a}\right)^{1-n} \frac{\cos\left[(1 - n)\varphi\right]}{1 - n} - k\frac{\rho^2}{2f} \tag{4.7}$$

where $-k\frac{r^2}{2f}$ is called focusing term or lens term. The phase corrector expression is basically the transformer after the substitutions: $a \leftrightarrow b$, $n \to 1/n$ and $(r, \theta) \to (\rho, \varphi)$. The physical dimensions (in μm) used to simulate numerically this transformation are:

L	λ	a	b	f [mm]
2000	0.6328	300	250	15

Table 4.1: Physical parameters for CST simulation in μm in Figures 4.1 and 4.2

The sampling ratio is $dx = L/M = 2$ μm. Figure 4.1 exhibits a simulation of this phenomenon with $n = 2$. As expected the input intensity distribution is mapped onto a π arc.

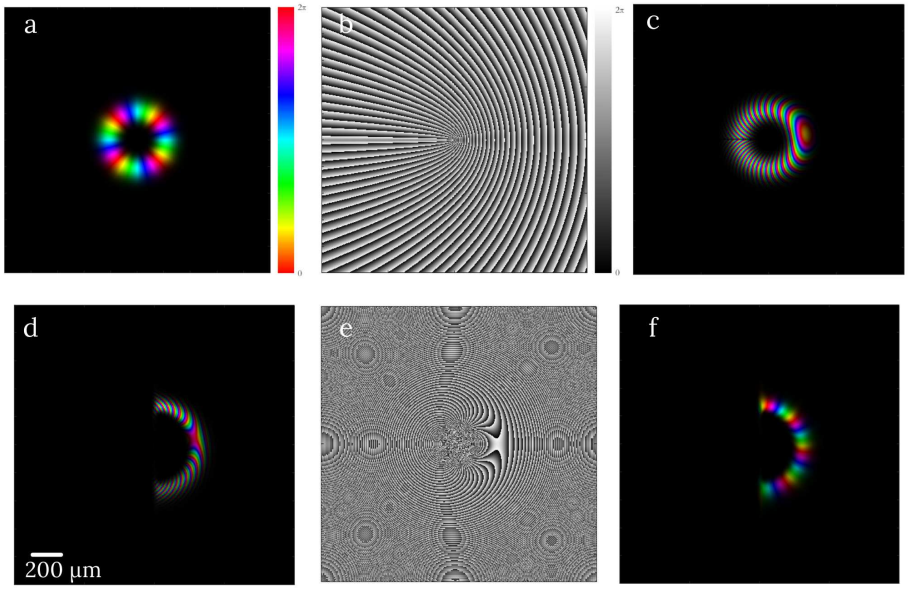

Figure 4.1: (a) Input $\mathrm{LG}_{(0,4)}$, $w_0 = 150\,\mu$m, (b) transformer phase pattern, (c) propagation at $z = 0.1f$, (d) beam at $z = f$, (e) phase-corrector, (f) beam after the phase-corrector. For the transformation parameters see Table 4.1. In (a, c, d, f) brightness and colours refer to intensity and phase, respectively.

4.2 The OAM multiplier

The OAM multiplication consists in projecting the initial phase distribution of an input beam into n complementary circular-sector parts, having each one the same phase distribution equal to the initial one [5]. Therefore the phase pattern of the multiplier Ω_M is the superposition of n circular-sector transformations $\Omega_S^{(j)}$ mapping the input beam over the corresponding circular sectors with amplitude $2\pi/n$ and centered on $(j-1)\frac{2\pi}{n}$ with $j = 1, ..., n$. The analytic form is:

$$\Omega_S^{(j)}(r,\theta) = \frac{kab}{f}\left(\frac{r}{b}\right)^{1-\frac{1}{n}} \frac{\cos\left[\left(1-\frac{1}{n}\right)\theta + (j-1)\frac{2\pi}{n}\right]}{1-\frac{1}{n}} - k\frac{r^2}{2f} \tag{4.8}$$

and in particular the phase pattern of the multiplier is:

$$\Omega_M(r,\theta) = \arg\left(\sum_{j=1}^{n} e^{i\Omega_S^{(j)}}\right) \tag{4.9}$$

The phase-corrector will have the same form of the CST in Eq. (4.7) because the inverse transformation is the same for all the contributions. Now we will see some simulations of this technique. The first example shows the multiplication of a factor $n = 2$. In this case the physical parameters of the simulations will be the same as those of the CST in Fig. 4.1, with the difference that the input OAM beam has topological charge $\ell = 2$. The parameter n is set $n = 2$, therefore the input beam is projected into two π arcs which are then combined together providing an output beam with $\ell = 4$ (figure 4.2).

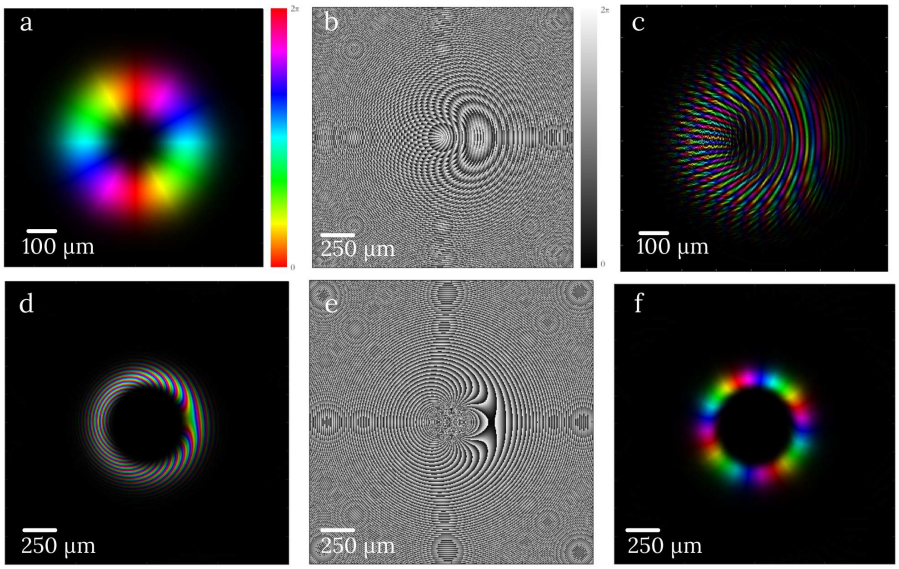

Figure 4.2: (a) Input $LG_{(0,2)}$, $n = 2$ $w_0 = 150$ μm, (b) transformer phase pattern, (c) propagation at $z = 0.1f$, (d) beam at $z = f$, (e) phase-corrector, (f) beam after the phase-corrector. For the transformation parameters see Table 4.1. In (a, c, d, f) brightness and colours refer to intensity and phase, respectively

We can clearly change the output modifying the ℓ and n parameters. It is worth noting that the multiplication is independent of the ℓ parameter, therefore the n parameter is "encoded" into the transformer and phase corrector. In the following image we show the duplication of a beam with $\ell = 5$.

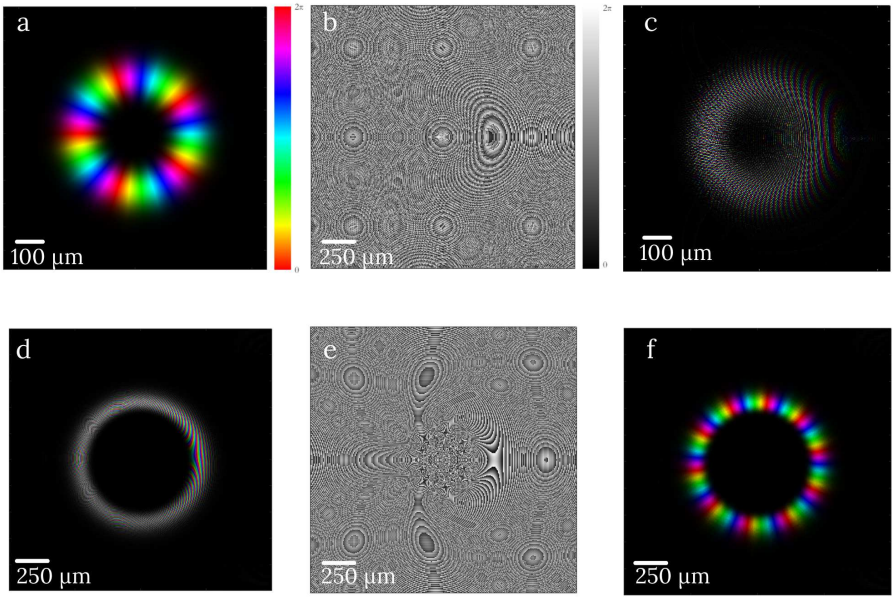

Figure 4.3: (a) Input $LG_{(0,5)}$, $n = 2$, $w_0 = 150$ μm, (b) transformer phase pattern, (c) propagation at $z = 0.1f$, (d) beam at $z = f$, (e) phase-corrector, (f) beam after the phase-corrector. The transformation parameters are: a=400 μm, b=350 μm and f=10 mm. In (a, c, d, f) brightness and colours refer to intensity and phase, respectively

In figure 4.4 we increase the parameter n to three. This makes more evident the deformation of the output beam as shown in the following, the physical parameters used are the same of figure 4.1. This distortion is caused by the twisted wavefront

of the input OAM beam. In fact, the phase patterns in eqs. (4.6), (4.7), (4.8) and (4.9) are calculated in the stationary phase approximation, assuming a planar phase front in the input. However OAM beams have a peculiar azimuthal phase, which affects the final intensity distribution of the transformed beam. This effect can be mitigated and the conversion efficiency can be optimized by properly designing the transformation optics in terms of the focal length f and design parameters a and b [5]. Arranging the previous parameters to f=10 mm, a=500 μm and b=350 μm we can reduce the deformation obtaining figure 4.5.

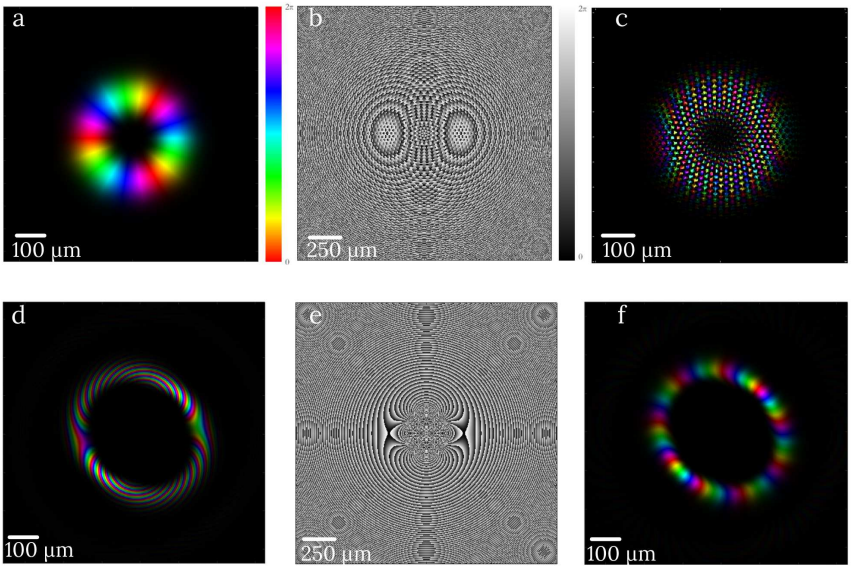

Figure 4.4: (a) Input $LG_{(0,3)}$, $n = 3$, $w_0 = 150$ μm, (b) transformer phase pattern, (c) beam at $z = 0.1f$, (d) $z = f$, (e) phase-corrector, (f) after the phase-corrector. For the transformation parameters see Table 4.1. In (a, c, d, f) brightness and colours refer to intensity and phase, respectively

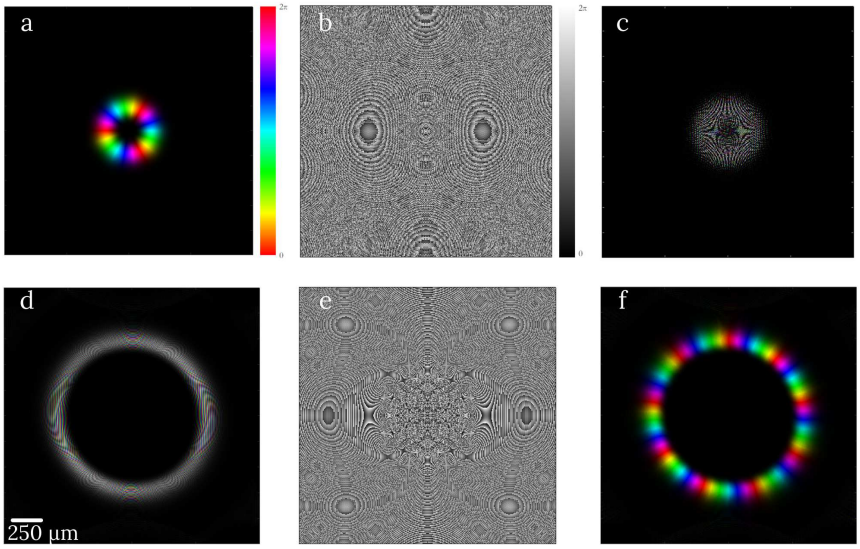

Figure 4.5: (a) LG beam input with $m = 3$, $p = 0$, $n = 3$, $w_0 = 150$ μm, (b) transformer phase pattern, (c) beam at $z = 0.1f$, (d) $z = f$, (e) phase-corrector, (f) after the phase-corrector. The transformation parameters are: a=500 μm b=350 μm and f=10 mm. In (a, c, d, f) brightness and colours refer to intensity and phase, respectively

The OAM divider

It is also possible to divide a beam into a bunch of n beams with OAM equal to $1/n$ of the input OAM. This kind of transformation is essentially a theme variation of the previous one. In particular, it is possible to divide an input OAM into n new non overlapping beams with a rescaled phase. We are not going to report all the analytical expressions because we will not simulate an OAM division. However it is meaningful to mention that an OAM can be de-multiplied in equal portions, as shown in [5].

Conclusions

We showed both analytically and numerically that it is possible to manipulate light that carries OAM by means of optical phase elements implementing conformal optical transformations. In particular, we have studied the cases of log-pol and circular-sector transformations. We solved numerically, through the fast Fourier transform, the Fresnel-Kirchhoff diffraction formula, producing a simulation of the field after the first phase element and the phase-corrector. The demultiplexing as a sorter of OAM modes was also discussed as an application of the log-pol mapping. For the CST, the application was the multiplication of factor n of the input OAM mode. The results of numerical simulations exhibit a good agreement with what is expected form the theory, and confirm the validity and effectiveness of conformal mappings for OAM manipulation.

Some applications of this technology concern mode division multiplexing through optical fibres [18], [3] and free space optical communication [12], [9] although the relevant recent results improve the actual transmission rate only for short distances (<100 km) communications. Possible applications of the OAM multiplication are: optical operations on OAM, routing/switching among OAM channels, optical computation, multicasting.

The central issue of OAM communications is the crosstalk due to mode coupling, other challenges include compact integrated OAM multiplexer, mode filter, demultiplexer as well as OAM mode converter components [19]. Quoting M.J. Padgett: "Perhaps the most active, and arguably most contentious, of OAM sub-field of recent years has been the application of OAM to optical communication" [14].

The optical elements implementing conformal transformations are usually realized with diffractive optical elements (DOEs) or with spiral phase plates and q-plate technology [11]. An other way to generate and modify OAM beams is the spatial light modulator (SLM) [14]. The latest way to shape light uses metasurfaces. These are made of subwavelength-structures patterned on an interface, by appropriately adjusting their size, orientation, geometry and arrangement, one can control/change the fundamental properties of incident light and thus modify the wavefront according to desired specifications [8].

A Appendix

A.1 The stationary phase approximation

$$\int_{\mathbb{R}^n} g(x)e^{ikf(x)}dx \approx \sum_{x_0\in\Sigma} e^{ikf(x_0)}\frac{1}{\sqrt{|\det(\mathrm{Hess}(f))|}}e^{\pi i/4\mathrm{sgn}(\mathrm{Hess}(f))}\left(\frac{2\pi}{k}\right)^{n/2} g(x_0) \qquad k\to\infty \tag{A.1}$$

with 'sgn' the signature of the Hessian, Σ the set of nondegenerate critical points $\det\{(\mathrm{Hess}(f(x_0)))\}\neq 0$.

A.2 Holomorphic functions and conformal transformations

Definition A.2.1 (Holomorphic function) *A function $f : D\subset\mathbb{C}\to\mathbb{C}$, $f = u(x,y)+iv(x,y)$ is holomorphic if and only if $u = \mathrm{Re}f$ and $v = \mathrm{Im}f$ are both C^1 and satisfy the Cauchy–Riemann equations*[1]*:*

$$\begin{cases} \frac{\partial u(x,y)}{\partial x} = \frac{\partial v(x,y)}{\partial y} \\ \\ \frac{\partial u(x,y)}{\partial y} = -\frac{\partial v(x,y)}{\partial x} \end{cases} \iff \frac{\partial f}{\partial \bar{z}} = \frac{1}{2}\left(\frac{\partial}{\partial x}+i\frac{\partial}{\partial y}\right)f = 0 \tag{A.2}$$

Definition A.2.2 (Anti-holomorphic function) *A function $f : D\subset\mathbb{C}\to\mathbb{C}$, is anti-holomorphic if its conjugated $\bar{f} = u(x,y)-iv(x,y)$ is holomorphic, therefore if:*

$$\begin{cases} \frac{\partial u(x,y)}{\partial x} = -\frac{\partial v(x,y)}{\partial y} \\ \\ \frac{\partial u(x,y)}{\partial y} = \frac{\partial v(x,y)}{\partial x} \end{cases} \iff \frac{\partial f}{\partial z} = \frac{1}{2}\left(\frac{\partial}{\partial x}-i\frac{\partial}{\partial y}\right)f = 0 \tag{A.3}$$

Definition A.2.3 (Conformal transformation) *In the euclidean space V, a non-degenerate linear transformation $T : V\to V$ is conformal if it preserves the angles, so that $\vec{u},\vec{v}\in V$:*

$$\frac{\vec{Tu}\cdot\vec{Tv}}{|\vec{Tu}||\vec{Tv}|} = \frac{\vec{u}\cdot\vec{v}}{|\vec{u}||\vec{v}|} \tag{A.4}$$

A.3 The general solutions of Laplace Equation

In polar coordinates (r,θ) we have:

$$\nabla^2 = \frac{1}{r}\frac{\partial}{\partial r}\left(r\frac{\partial}{\partial r}\right)+\frac{1}{r^2}\frac{\partial^2}{\partial\theta^2} \tag{A.5}$$

[1] A shorter form of C-R equations is the Wirtinger operator shown above

therefore (2.8) becomes:

$$\left[r\frac{\partial}{\partial r}\left(r\frac{\partial}{\partial r}\right)+\frac{\partial^2}{\partial\theta^2}\right]\Omega=0 \tag{A.6}$$

Assuming $\Omega(r,\theta)=R(r)\Theta(\theta)$ we have:

$$\frac{1}{R}\nabla_r^2 R+\frac{1}{\Theta}\nabla_\theta^2\Theta=0 \quad \Rightarrow \quad \begin{cases}\frac{1}{\Theta}\nabla_\theta^2\Theta=-m^2\\ \\ \frac{1}{R}\nabla_r^2 R=m^2\end{cases} \tag{A.7}$$

The first differential equation is easy to solve and the solutions are $\Theta(\theta)=A_1e^{\pm im\theta}$, whereas the second is an Euler equation. The calculations get:

$$r^2R''+rR'-Rm^2=0 \tag{A.8}$$

applying the change of variables: $z(t)=R(e^t)$ it is easy to obtain: $R(r)=A_2r^{\pm m}$ resulting in:

$$\Omega(r,\theta)=A_1A_2r^{\pm m}e^{\pm im\theta} \tag{A.9}$$

A.4 IR and TF sampling

The transfer function (1.18) is a function of frequency, so extracting the phase gives:

$$\phi=-i\pi\lambda z(f_u^2+f_v^2) \tag{A.10}$$

For a uniform sample interval of f_u the criterion for an unambiguous representation of the phase, when it is encoded in a modulo 2π, format can be written as:

$$\Delta f_u\left|\frac{\partial\phi}{\partial f_u}\right|\leq\pi \tag{A.11}$$

This expression states that the maximum change in the absolute phase must be no more than π between any two adjacent samples. The maximum slope occurs when f_u is a maximum (f_{umax}). Inserting this information into (A.10) and solving for Δf_u gives the following criterion for the sample interval:

$$\Delta f_u\leq\frac{1}{2\lambda z f_{umax}} \tag{A.12}$$

Assuming the frequency and spatial domain sampling are related through the

$$\Delta f_u=\frac{1}{L}\qquad |f_{umax}|=\frac{1}{2dx} \tag{A.13}$$

where L is the side length and dx is the sample interval in the spatial domain. Substituting these relations we have:

$$dx\geq\frac{\lambda z}{L} \tag{A.14}$$

The impulse response (1.16) has a phase:

$$\varphi=\frac{ik}{2z}\rho^2\qquad \rho=\sqrt{u^2+v^2} \tag{A.15}$$

Proceeding in the same manner as for the transfer function, the criterion for adequately sampling the impulse response is:

$$dx \leq \frac{\lambda z}{2|x_{max}|} \tag{A.16}$$

in our case $|x_{max}| = L/2$ resulting:

$$dx \leq \frac{\lambda z}{L} \tag{A.17}$$

Equations (A.17), (A.14) are essentially the opposite. Defining as before the $c = \lambda z/Ldx$ parameter the conditions of oversampling and undersampling are:

Regime	Phase sampling
$c < 1$	TF over IR under
$c = 1$	Identical
$c > 1$	TF under IR over

A.5 The LG beam terms

The terms of (1.23) are:

$$\begin{cases} C_{\mathrm{LG}(p,\ell)} = \sqrt{2p!/(\pi(p+|\ell|)!)} & \text{Normalization constant} \\ L_p^{|\ell|}(x) = \frac{x^{-|\ell|}e^x}{p!}\frac{d^p}{dx^p}(e^{-x}x^{p+|\ell|}) & \text{Rodrigues formula} \\ \zeta(z) = \tan^{-1}(z/z_R) & \text{Gouy phase} \\ z_R = \pi w_0^2/\lambda & \text{Rayleigh range} \\ w(z) = w_0\sqrt{1+(z/z_R)^2} & \text{Beam radius} \end{cases} \tag{A.18}$$

The Rodrigues formula describes the generalized Laguerre–Gauss polynomial of p (radial mode) and ℓ (angular mode). The factor $e^{i\ell\theta}$ is what allows these beams to exhibit OAM. How does light with OAM looks like? A common laser has not OAM ($\ell = 0$) and is made up of plane waves in the far field, and if you point it towards a wall you see only a bright Gaussian-like spot. A light beam with OAM, instead, has twisted wavefronts rotating during propagation and resulting into a doughnut intensity distribution, due to the central dark phase singularity. In summary OAM beams are characterized by a helical phase form $\exp(i\ell\theta)$ with $(\ell = 0, \pm1, \pm2, ...)$, being ℓ the topological charge and θ the azimuthal coordinate.

Bibliography

[1] L Allen, MJ Padgett, and M Babiker. Iv the orbital angular momentum of light. *Progress in optics*, 39:291–372, 1999.

[2] Max Born and Emil Wolf. *Principles of optics: electromagnetic theory of propagation, interference and diffraction of light*. Elsevier, 2013.

[3] Nenad Bozinovic, Yang Yue, Yongxiong Ren, Moshe Tur, Poul Kristensen, Hao Huang, Alan E Willner, and Siddharth Ramachandran. Terabit-scale orbital angular momentum mode division multiplexing in fibers. *science*, 340(6140):1545–1548, 2013.

[4] Watnik AT. Doster T. Laguerre-gauss and bessel-gauss beams propagation through turbulence: analysis of channel efficiency. *Applied Optics (2016)*.

[5] Michele Massari Gianluca Ruffato and Filippo Romanato. Multiplication and division of the orbital angular momentum of light with diffractive transformation optics. *Light: Science & Applications (2019)*.

[6] Joseph W. Goodman. *Introduction to Fourier optics / Joseph W. Goodman*. Roberts Co. Publishers, Englewood, Colo, 3rd ed edition, c2005.

[7] W.J. Hossack, A.M. Darling, and A. Dahdouh. Coordinate transformations with multiple computer-generated optical elements. *Journal of Modern Optics*, 34(9):1235–1250, 1987.

[8] Mohammadreza Khorasaninejad, Wei Ting Chen, Alexander Y Zhu, Jaewon Oh, Robert C Devlin, Charles Roques-Carmes, Ishan Mishra, and Federico Capasso. Visible wavelength planar metalenses based on titanium dioxide. *IEEE Journal of Selected Topics in Quantum Electronics*, 23(3):43–58, 2016.

[9] Mario Krenn, Johannes Handsteiner, Matthias Fink, Robert Fickler, Rupert Ursin, Mehul Malik, and Anton Zeilinger. Twisted light transmission over 143 km. *Proceedings of the National Academy of Sciences*, 113(48):13648–13653, 2016.

[10] Martin P J Lavery, Gregorius C G Berkhout, Johannes Courtial, and Miles J Padgett. Measurement of the light orbital angular momentum spectrum using an optical geometric transformation. *Journal of Optics*, 13(6):064006, apr 2011.

[11] Martin P. J. Lavery, David J. Robertson, Gregorius C. G. Berkhout, Gordon D. Love, Miles J. Padgett, and Johannes Courtial. Refractive elements for the measurement of the orbital angular momentum of a single photon. *Opt. Express*, 20(3):2110–2115, Jan 2012.

[12] Zhang M. Li Y. et al. Lei, T. Massive individual orbital angular momentum channels for multiplexing enabled by dammann gratings. *Light Sci Appl*, 2015.

[13] Junchang Li, Zujie Peng, and Yunchang Fu. Diffraction transfer function and its calculation of classic diffraction formula. *Optics Communications*, 280(2):243–248, 2007.

[14] Miles J. Padgett. Orbital angular momentum 25 years on. *Opt. Express*, 25(10):11265–11274, May 2017.

[15] G. Ruffato, E. Rotunno, L.M.C. Giberti, and V. Grillo. Arbitrary conformal transformations of wave functions. *Phys. Rev. Applied*, 15:054028, May 2021.

[16] Gianluca Ruffato, Michele Massari, Giuseppe Parisi, and Filippo Romanato. Test of mode-division multiplexing and demultiplexing in free-space with diffractive transformation optics. *Opt. Express*, 25(7):7859–7868, Apr 2017.

[17] David George Voelz. *Computational fourier optics: A MATLAB tutorial*. Bellingham, Wash: SPIE Press., 2011.

[18] Jian Wang, Shuhui Li, Ming Luo, Jun Liu, Long Zhu, Chao Li, Dequan Xie, Qi Yang, Shaohua Yu, Junqiang Sun, Xinliang Zhang, William Shieh, and Alan E. Willner. N-dimentional multiplexing link with 1.036-pbit/s transmission capacity and 112.6-bit/s/hz spectral efficiency using ofdm-8qam signals over 368 wdm pol-muxed 26 oam modes. pages 1–3, 2014.

[19] Siyuan Yu. Potentials and challenges of using orbital angular momentum communications in optical interconnects. *Optics express*, 23(3):3075–3087, 2015.